Postprint of: Krasiński A., Numerical simulation of screw displacement pile interaction with non-cohesive soil, Archives of Civil and Mechanical Engineering, Vol. 14, iss. 1 (2014), pp. 122-133, DOI: 10.1016/j.acme.2013.05.010

NUMERICAL SIMULATION OF SCREW DISPLACEMENT PILE INTERACTION WITH NON-COHESIVE SOIL

Adam Krasiński[*)]
Gdansk University of Technology, ul. Narutowicza 11/12, 80-233 Gdansk, Poland

Abstract. A trial numerical simulation of screw displacement pile interaction with non-cohesive subsoil during the transfer of compression load is described. The simulation was carried out in an axisymmetric system using the Plaxis 2D-FEM computer programme. The technological phases of pile installation in the ground were numerically modelled using equivalent processes which provided similar effects to real technical actions. The results of the numerical calculations were verified by comparing with the load test results of a real pile in the field. The analysis shows that, apart from the technological elements, a proper numerical simulation of screw displacement pile interaction with non-cohesive soil also needs to take into account soil characteristics as defined in the critical state theory.

Keywords:
Pile, screw displacement pile, numerical simulation

1. Introduction

Numerical analysis of pile–soil interaction is a rather complex subject that is still being researched in geotechnical engineering. Problems appear when the numerical calculation results are verified by real field test results, as very often comparison of the results reveals significant discrepancies. One of the reasons for this could concern the method of modelling pile installation elements (processes) in numerical simulations. Other reasons might be connected with the constitutive model of soil and the values of geotechnical parameters used in the numerical analyses.

There are many technologies of pile installation, especially in cases of cast-in-situ piles. Piles can be created by boring into the ground with or without casing (using or not bentonite slurry), or by using a continuous flight auger (CFA piles). Vibro and Franki piles can be made by driving a steel tube into the soil and removing it after the concrete has set. A rarer method involves making the pile casing penetrate the soil by vibration or jacking. Finally, there are screw displacement piles (i.e. “Omega”, SDP, or “Atlas” piles, [1-3]). Thanks to its efficiency, this newest pile technology is becoming increasingly popular in practice.

The end result of each of the mentioned techniques can be a pile of the same geometrical and material properties (the diameter, length and stiffness or strength of the pile core). However,

[*)] PhD. Eng., corresponding author, e-mail: akra@pg.gda.pl, Tel. +48 58 347 10 44, Fax. +48 58 347 22 09, postal address: Gdansk University of Technology, Faculty of Civil and Environmental Engineering, ul. Narutowicza 11/12, 80-233 Gdansk, Poland.

in terms of soil interaction these piles may vary significantly. The technology of pile installation can substantially affect the density and stress conditions in the surrounding soil. Bored pile technologies usually cause a reduction of soil density and stress, whereas displacement piles (driven and screw) cause an increase in such values. Moreover, in cases of driven piles the biggest installation influence occurs in the soil under the pile base, whereas in the case of screw displacement piles the biggest changes occur in the soil around the pile shaft.

The above mentioned pile installation effects should also be taken into account in numerical simulations. It is relatively simple to numerically simulate the installation of a bored pile. Simulations of displacement piles are more difficult. Successful numerical simulations of bored piles and precast driven, vibro-driven and jacked piles have been carried out, e.g. by Mahutka et al. [4] or Henke and Grabe [5]. On the other hand, there is little information in literature on numerical simulations regarding screw displacement piles. Though well known, the numerical analyses of Basu and Prezzi [6] are limited to the problem of contact between narrow non-cohesive soil section and a shaft of the screw displacement auger and pile.

In this paper the results of a numerical simulation of a screw displacement pile (SDP) interacting with a non-cohesive soil are described. Particular emphasis was placed on modelling the main technological phases of pile installation as well as the final static pile load phase. The modelling and calculations were carried out using the axisymmetric system and the Plaxis 2D [7] computer programme with standard Hardening Soil (HS) and Mohr–Coulomb (CM) soil models. Chosen for the analysis was a real SDP pile, made and tested in the field. The final numerical calculation results were compared with the results of a field pile test. On the basis of this comparison appropriate conclusions were drawn.

2. Short characteristic of screw displacement piles

Despite many types of screw displacement pile technology, the basic idea of installing these piles is approximately the same. Fig. 1 presents the phases of installing a Screw Displacement Pile (SDP). The installation begins with the special displacement auger penetrating the subsoil. The auger's construction and shape mean that during rotation and penetration it horizontally displaces the soil on all sides to leave a cavity for the pile. During the next phase, the auger is unscrewed while concrete is simultaneously poured in under pressure. Immediately after concreting, the pile reinforcement is inserted by means of vibration.

Great soil resistances occur during auger penetration, especially in non-cohesive soils, and therefore very massive drilling machines with high torque need to be used. High soil resistances during installation is one of the greatest problems in screw displacement pile technology. Investigations are still ongoing to find optimal auger shapes improve screwing techniques with regard to soil resistance. Screwing resistances currently limit SDP pile diameters (to a maximum of 600 mm) and bearing lengths in the soil. Hence, their designed bearing capacities are also limited to 1000–1500 kN. On the other hand, SDP piles have a significantly greater bearing capacity than bored piles of the same geometric parameters, working in the same soil conditions.

Once installed, SDP piles interact very well with non-cohesive soils. Moreover, installation is ecological and cost effective.

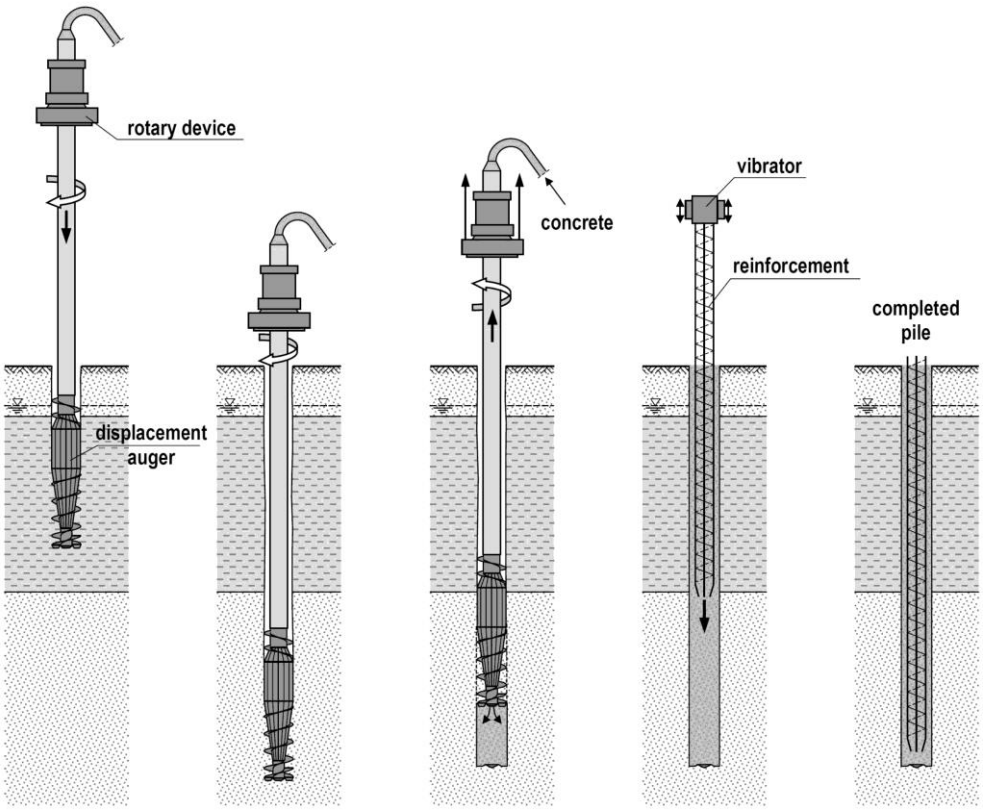

Fig. 1. Phases of SDP pile installation

3. SDP pile used in numerical analysis

The SDP pile chosen for the numerical simulation was one of four that had been tested in a field test site in the Vistula delta region of northern Poland for research project. Preliminary boreholes and CPTU tests were carried out to determine the structure and geotechnical parameters of the subsoil. CPTU tests were exactly in those places where the test piles were next installed. Approximately three weeks after installation, secondary CPTU tests were conducted at distances of 0.30 m from the pile shafts. All four piles were instrumented and had the following parameters: diameter D = 360 mm and length L = 7.0–9.0 m.

The geotechnical subsoil structure of the investigated site was typical for pile foundations. A layer from the ground level to a depth of 1-1.5 m was sandy. Next, to a depth of about 4.5 m, there was an organic layer of peat and mud. And below that there were layers of non-cohesive bearing soils: dense sandy gravels and medium dense fine sands and medium sands. Down to about 0.8 m the subsoil was fully saturated. A typical soil profile with q_c CPTU cone resistances measured before and after pile installation is presented in Fig. 2. One may note that after pile installation there was an increase of q_c resistances in the region around the pile, but under the pile base that increase was not very high. The same phenomenon was observed with regard to the other three tested pile installations. This allowed us to conclude that screw displacement piles mainly affect the soil conditions (density and stress level) around the pile shaft.

The four piles were next subjected to static load tests. Each pile was equipped with five vibrating wire extensometers to measure the axial force distribution along the pile core during successive static load steps. Much has already been written about this particular instrumentation, e.g. [8-10], thanks to which, apart from information about the load and settlement of the pile head, it is possible to determine how much of the load is borne by friction of soil layers along the pile shaft and how much by soil resistance under the pile base. Fig. 2 and 3 present the results of the SDP-b3 pile test after the interpretation of extensometer measurements. A more detailed description of the results of all the pile tests in this field site is found in the author's papers [11-13].

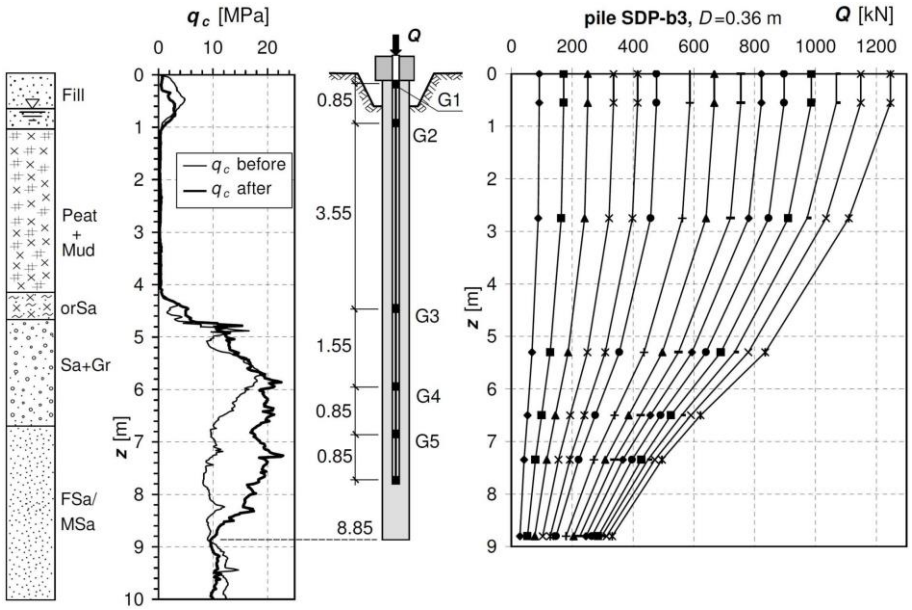

Fig. 2. CPTU test results regarding subsoil and axial force distribution along pile shaft during static load tests of pile SDP-b3

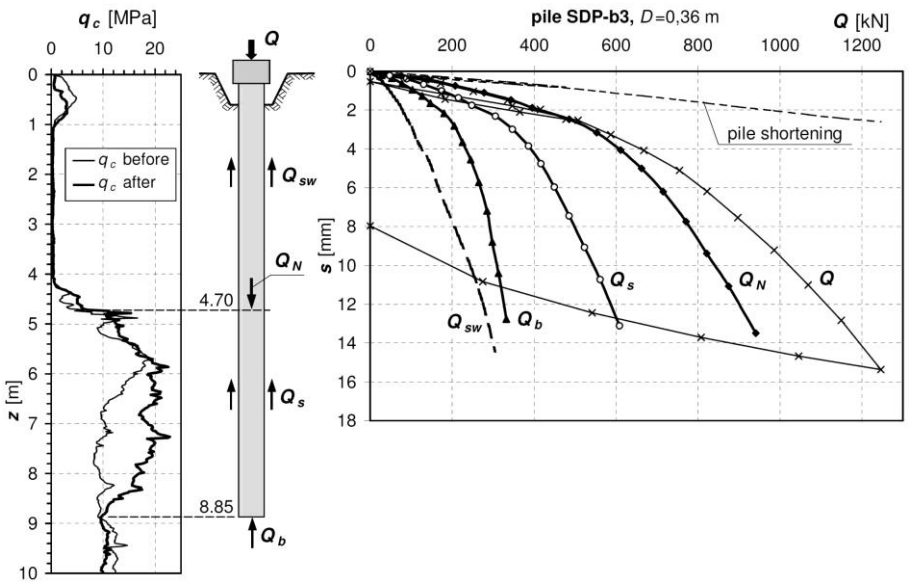

Fig. 3. Diagrams of pile SDP-b3 load-settlement with pile shaft and pile base resistances shown separately

4. Numerical modelling

The numerical analysis was treated as an initial-boundary problem and modelled using the axisymmetric system. A single cylindrical concrete pile located in a coordinate system vertical axis and working in subsoil layers was assumed. The geometry and mesh discretisation for the Plaxis code calculations are presented in Fig. 4.

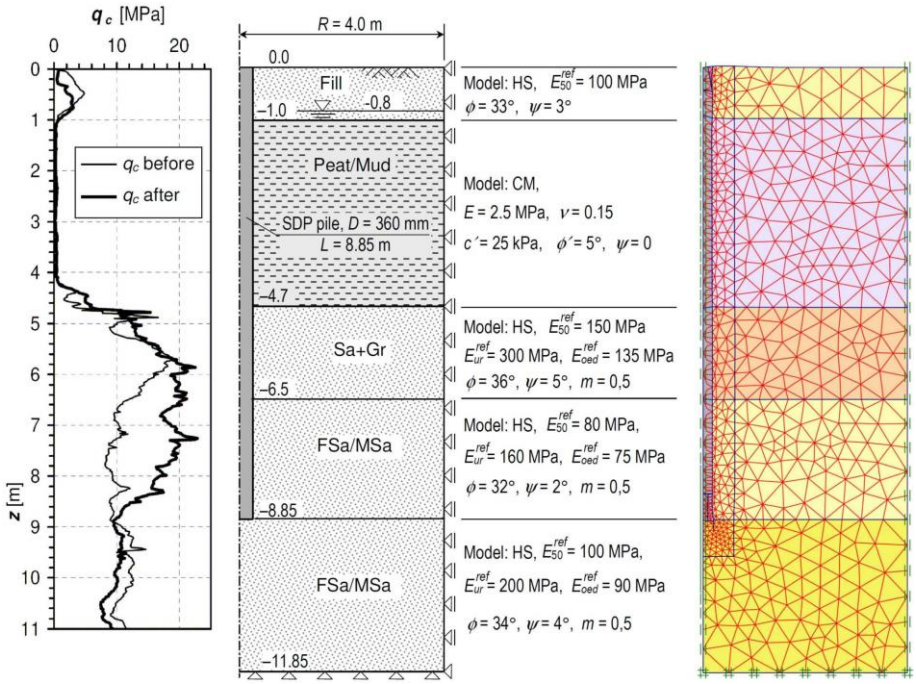

Fig. 4. Geometry and mesh discretisation in an axisymmetric system

The mesh was constructed out of 15-node triangular elements. Mesh discretisation immediately around the pile shaft and base was very fine, whereas in other areas it was medium. Optimal mesh element density was determined by trial. Along the border between the pile shaft and soil body, interface elements were applied with factor R_{int} = 1. It was assumed that in the case of cast-in-situ piles, the friction coefficient between non-cohesive soil and the pile shaft can be equal to the tangent of the soil internal friction angle $\mu = \mathrm{tg}\phi$. For the organic soil layers a Mohr-Coulomb (MC) model was applied, whereas for the sandy layers a Hardening Soil model [14] was used together with the exponential law of soil compressibility. The soil conditions were assumed to be normally consolidated.

Most of the geotechnical parameters of the soil were defined on the basis of CPTU tests using interpretation methods proposed by Lunne et al. [15]. Others, e.g. dilatancy angle and Poisson's ratio, were assumed on the basis of experience. The soil parameter values used in the numerical calculation are shown in Fig. 4.

After defining of the geometry and setting the initial stress state in the subsoil, the subsequent technological stages of pile installation and finally the phase of pile load were modelled.

4.1. Phase I – pile soil cavity formation by displacement auger

The insertion of a drilling tool (displacement auger) into the ground is a complex process and very difficult to replicate in model form. Nevertheless, we should note that the main task of the auger is to create the hole by radially displacing the soil and we are only interested in final effect of this process. It was assumed, that similar effect can be obtained using the process of axisymmetric cavity expansion (e.g. [16-18]).

To start cavity expansion using the Plaxis code, an initial borehole was modelled with an r_0 radius, which was equal to $D/4 = 0.09$ m, where D was the auger and pile diameter. The value of r_0 was selected after trials regarding its influence on the final result of numerical calculation. With the initial hole insertion, a simultaneous cavity expansion process was started, and it was finished when the radius was $r = D/2 = 0.18$ m. Soil displacement on the upper and lower ends of the cavity was triangular and 0.5 m high. This was so as to eliminate any unwanted finite element deformations in the mesh area around both ends of the cavity. In the lower section the displacement shape additionally corresponded to the shape of the auger. In order to obtain a cylindrical shape for the pile shaft, the missing end fragments in calculation phase III were obtained by turning the soil material into concrete. The method of modelling phase I is shown in Fig. 5. The augur's soil displacement caused a large increase of stress in the area around the cavity. The field of radial effective stress $\sigma'_{x\text{-}x}$ and its distribution in two selected cross-sections, A-A and B-B, are shown in Fig. 5.

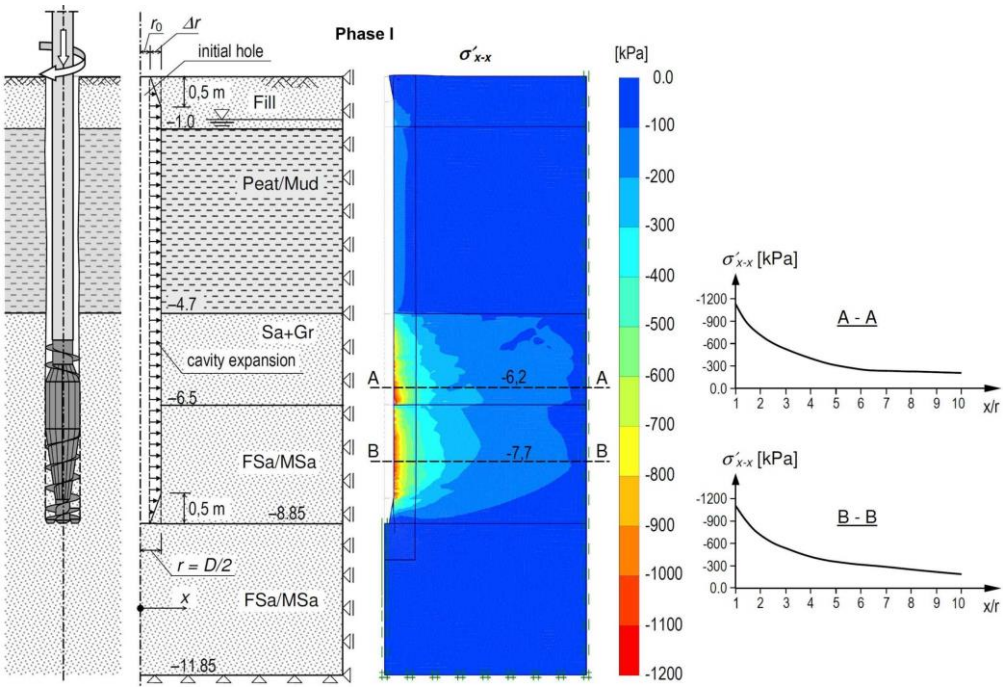

Fig. 5. Phase I model with numerically calculated component radial effective stress distribution in the soil $\sigma'_{x\text{-}x}$

4.2. Phase IIa and IIb – unscrewing the auger and concreting the pile shaft

Unscrewing the auger and concreting the pile shaft is an important technological stage that could not be ignored in the model. During unscrewing, the vacated cavity is immediately filled with a concrete mixture under pressure, which prevents it from collapsing. In practice the pressure of the concrete mixture is regulated by the pumping machine. However, once the auger is completely removed and the reinforcement, using the vibration method, introduced, the pressure of the pump applying the concrete is significantly reduced. It was therefore assumed that only the hydrostatic pressure of the concrete mixture would be permanent. As a result, relaxation occurs in the surrounding soil in relation to the state immediately after cavity completion.

The phase of filling the cavity with a concrete mixture was modelled using radial horizontal stress $p_{cs,}$ working on the cavity wall from the inside, and vertical pressure p_{cb}, affecting the bottom of the cavity. The value of p_{cs} pressure was taken to be equal to the hydrostatic pressure of the concrete mixture at a given depth. The concrete mixture was assumed to be a liquid with weight density γ'_b = 25 – 10 = 15 kN/m^3 (minus the buoyancy of water). The value of pressure at the bottom of the cavity, $p_{cb,}$ in phase IIa was taken to equal 1800 kPa, as defined through trials and considerably greater than the hydrostatic pressure of the concrete. Thus the vertical load of the auger bearing down on the bottom of the cavity during drilling was taken into account, although it could not be included in phase I of modelling. In phase IIb the vertical load on the bottom of the cavity was reduced to the value of concrete mixture hydrostatic pressure. Thanks to this operation, the effect of initial (preconsolidation) pressure of the soil under the pile base was obtained. Calculation tests showed that this effect had a considerable influence on soil resistance under the pile base during the load test phase. The method of modelling phase II is presented in Fig. 6, which also shows the numerically obtained radial effective pressure distribution $\sigma'_{x\text{-}x}$ in the soil.

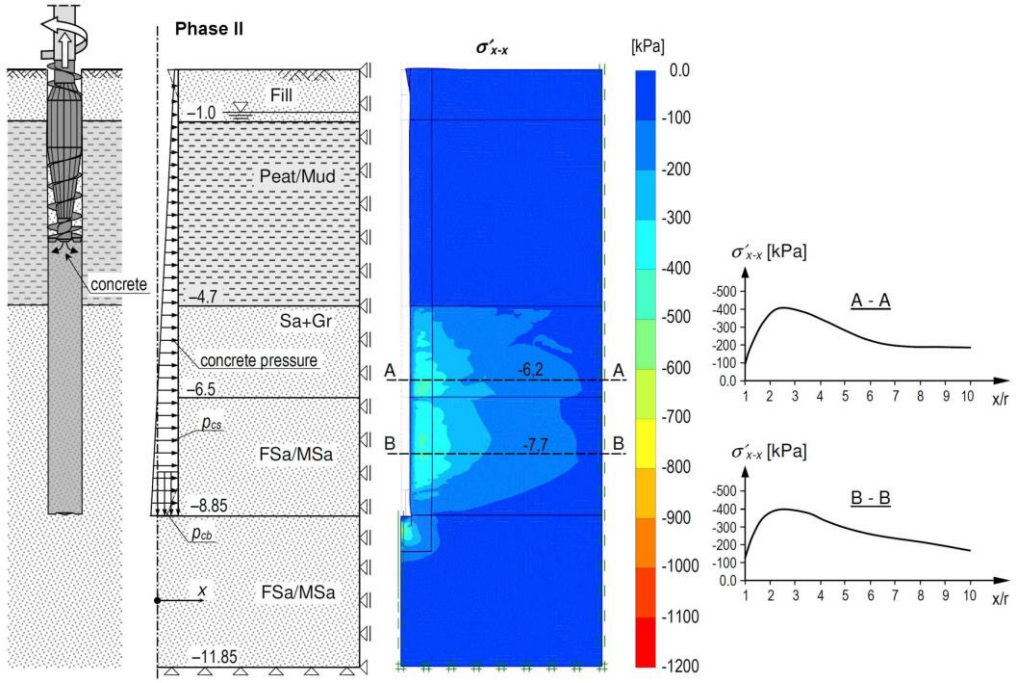

Fig. 6. Phase II model with calculated radial effective pressure distribution in the soil $\sigma'_{x\text{-}x}$

In phase II there was a decrease of stress in the soil around the cavity. In the soil next to the pile shaft (x/r = 1) the radial effective pressure $\sigma'_{x\text{-}x}$ was equal to that of the concrete mixture p_{cs}. Proceeding away from the pile boundary, the soil pressure $\sigma'_{x\text{-}x}$ first increases to a maximum value of approximately 400 kPa, at a distance of approximately x/r = 2.5, and then decreases. After phase I, at the distance x/r = 2.5 the stress value $\sigma'_{x\text{-}x}$ in cross-sections A-A and B-B was approximately 600 kPa, and therefore phase II reduced it by about 30%.

4.3. Phase III – hardening of concrete in the pile core

In phase III the inside of the cavity was filled with an elastic material with the full strength of concrete. Simultaneously, interface elements were activated and concrete mixture pressure effects p_{cs} and p_{cb} of the previous phase were deactivated. The possible phenomenon of concrete shrinkage was ignored in this model. As a result of this operation the state of stress did not significantly change in relation to the state after phase II, as is shown in Fig. 7.

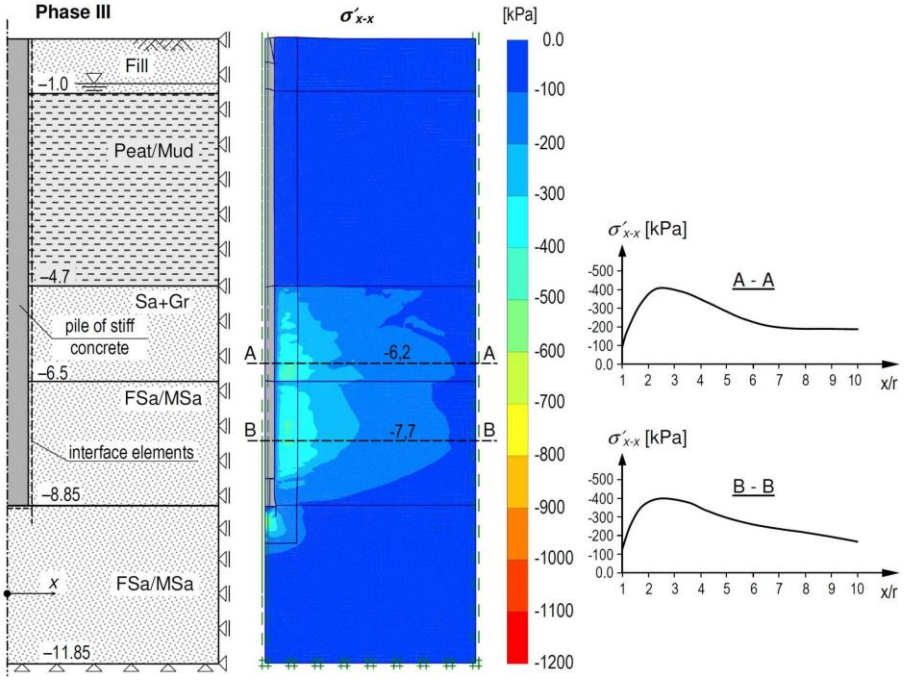

Fig. 7. Phase III model with calculated radial effective pressure distribution in the soil $\sigma'_{x\text{-}x}$

4.4. Phase IV – pile load test

The final calculation phase concerned modelling the pile load test. This was achieved by applying vertical stress p_v to the pile head. The stress value was determined by trial so that the final calculation results would vertically displace the pile by circa 10% of its diameter D. In this case the final value of stress p_v was 23.0 MPa.

Fig. 8 presents a diagram of the phase IV model as well as the numerically calculated radial $\sigma'_{x\text{-}x}$ and vertical $\sigma'_{y\text{-}y}$ effective stress distributions in the soil. These distributions correspond to the final value of the pile load. Fig. 9 presents the numerically obtained vertical

displacements field as well as the distribution of these displacements in cross-sections A-A and B-B. These distributions also correspond to the final value of the pile load.

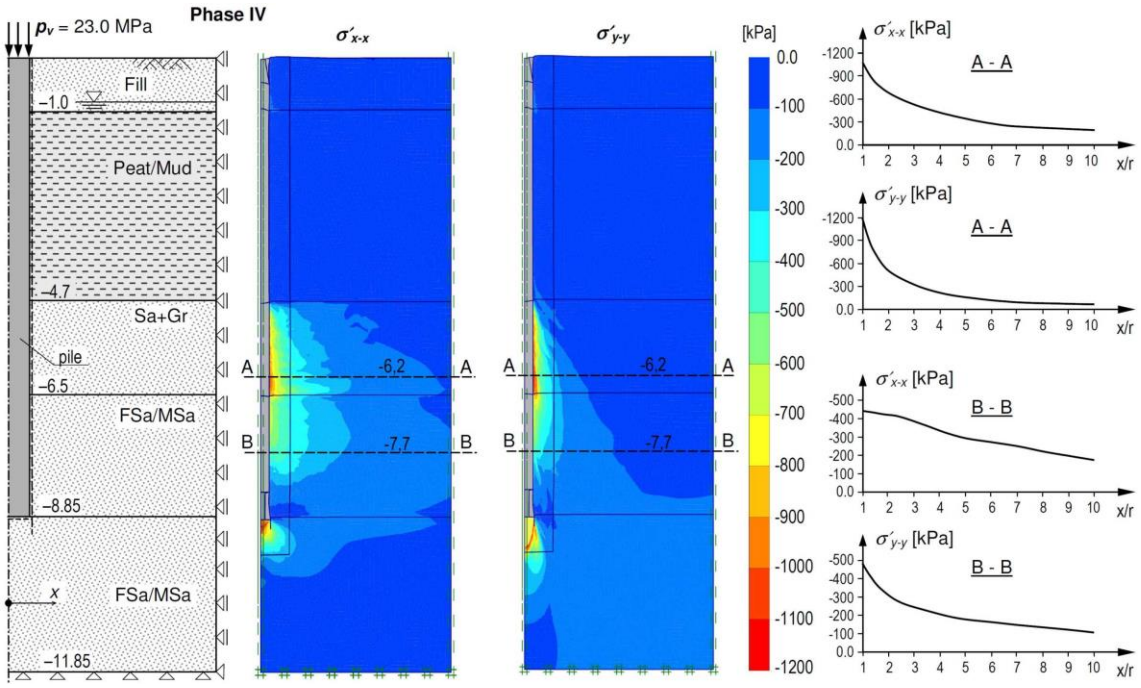

Fig. 8. Phase IV model with calculated radial and vertical effective stress distributions in the soil

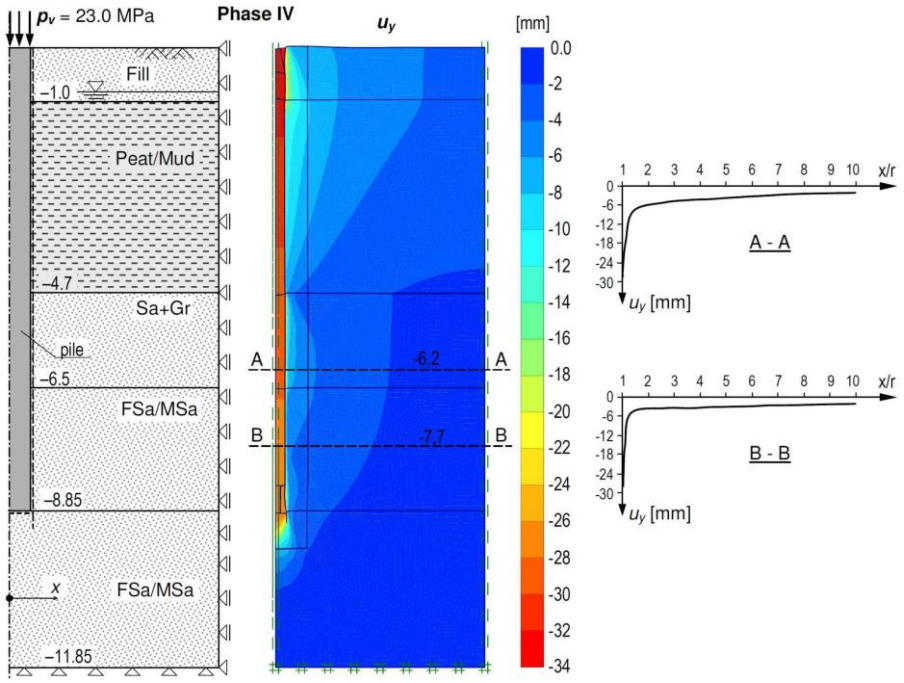

Fig. 9. Phase IV – vertical distributions field obtained from numerical calculations

4.5. The calculation process

Due to the fact that the analysed subject caused large deformations in the finite element mesh, the calculations were carried out using the 'updated mesh' option. Other calculation process parameters, e.g. permissible error and the number of iteration steps, were complied with standard Plaxis programme options.

5. Analysis of calculation results

The most important subject of the final analysis were the pile load-displacement relation curve and the curves of component forces carried by soil along the pile shaft and under the base. These relate to forces Q_N, Q_s, $Q_{b,}$, defined in the pile core deformation analysis. For this purpose the pile was divided into several sections and on the basis of the calculated deformations in each section, assuming the longitudinal pile core stiffness to be EA, the relevant Q_i force was obtained. These numerical results are compared with the field test results in Fig. 10.

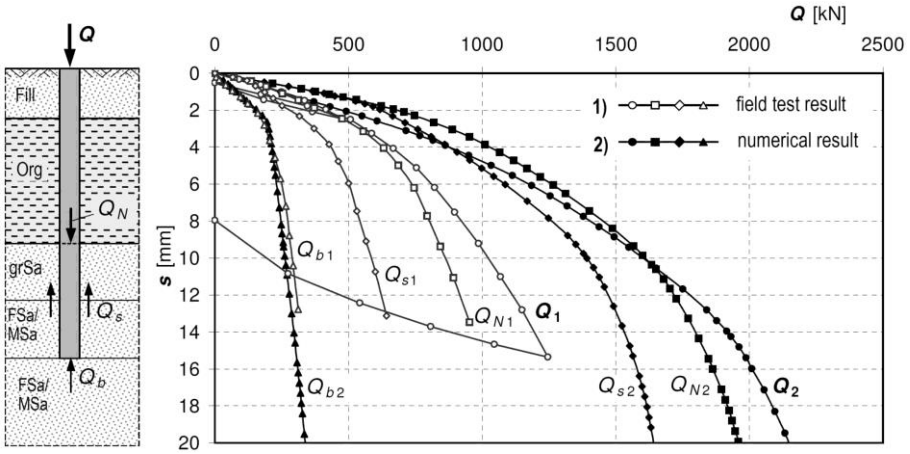

Fig. 10. Numerical pile load-displacement curves compared with field test result curves

We may note that the numerical calculations considerably exceed the field test results. This is particularly noticeable in Q_{s2} pile shaft resistance. One the other hand, Q_b pile base resistance corresponds well with the field test results.

Subsequent analysis showed that the Q_s shaft resistance discrepancy was due to the fact that the numerical calculations had not taken into account pile auger rotation, or rather the effect this rotation has on the surrounding soil. The importance of this phenomenon has been pointed out by Basu and Prezii [6]. In their numerical analyses, using a quasi-axisymmetric system, they observed that very large radial stress following cavity expansion is rapidly reduced as a result of auger rotation and vertical movement. A typical result of their analyses is presented in Fig. 11.

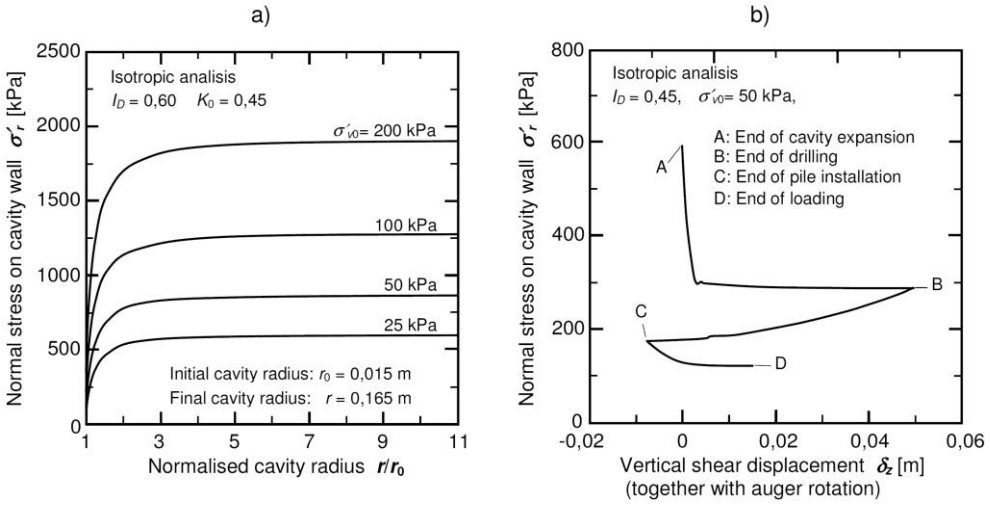

Fig. 11. Analysis results of Basu and Prezzi [6]: (a) radial stress generation in the soil during cavity expansion, (b) changes occurring during successive stages of screw pile installation

These radial stress changes were obtained not only by modelling auger rotation, but above all thanks to the application of an appropriate model of non-cohesive soil. In their case it was the Manzari and Dafalias [19] model, whose material description includes critical state theory (Rowe [20], Bolton [21]). According to this theory, non-cohesive soil with an initial state of density (void ratio e_0) and mean effective stress p'_0, progresses during shearing to a state of critical density, i.e. to critical void ratio e_{cs}. The value of this ratio depends on the type of soil (granularity) and stress level. With the increase of stress, the value of e_{cs} diminishes. This relation is, for example, defined in an equation by Biarez and Hicher [22]:

$$e_{cs} = e_{ref} - \lambda \cdot \log(p'/p_{ref}) \tag{1}$$

where: λ – material constant, obtained from experiments

p' – mean effective stress in soil

e_{ref}, p_{ref} – critical state line reference values, obtained from experiments

Even in dense soils, when the p' stress value is high, critical void ratio e_{cs} is usually lower than initial void ratio e_0, which means that during shearing only contractancy occurs.

When the soil is in a critical state, its strength parameters undergo modification: internal friction angle ϕ achieves value ϕ_{cs}, and therefore dilatancy angle ψ approaches zero value. The relation between internal friction angle ϕ and initial void ratio e_0 is expressed, for example, in an equation by Biarez and Hicher [22]:

$$\tan\phi = (e_{cs}/e_0)^m \cdot \tan\phi_{sc} \tag{2}$$

where: m – material constant, obtained from experiments.

From equations (1) and (2) it follows that the peak value of internal friction angle ϕ depends on the soil density and the mean effective stress.

As is now commonly known, soil stiffness is also considerably reduced during shearing: E and G moduluses.

During auger penetration, its rations and downward displacement cause full critical state conditions of the soil in contact band around the auger shaft. We need to additionally take into account that with the spreading of soil radial stress increases, while in the soil around the augur itself contractancy dominates. Thus the mechanical parameters of the soil, ϕ and ψ as well as E and M, are reduced in relation to initial values. In effect, significantly lower soil stresses are generated near a rotating augur than if there was no augur rotation.

6. Second, modified calculation approach

Modelling augur rotation is not possible in an axisymmetric system. Nor would it be an easy task in a 3D or plane strain system. Moreover, one should bear in mind that augur rotations would have to occur simultaneously with the cylindrical spreading of the soil.

On the other hand, we should also remember that here the technological phases of the screw displacement pile are only intermediate stages leading to an end state of stresses in the soil, and it is only here that a simulation should be as similar as possible to the actual conditions. Assuming that a rotating augur puts surrounding soil into a full critical state, it was decided that a similar end effect could still be obtained using the axisymmetric system without modelling the augur rotation but by modifying the mechanical parameters of the soil. Therefore an additional zone (zone 2) of $3r$ around the pile shaft was introduced to the geometric model. The soil in zone 2 had lowered mechanical parameters in the HS model, roughly corresponding to the critical state parameters. Depending on the soil layer, internal friction angle ϕ was lowered to 32° and 31°, and dilatancy angle ψ to 2° and 1° (Fig. 12). A very large, fivefold reduction was made to the E_{50}^{ref} modulus. The same reduction was made in relation to the secondary modulus, $E_{ur}^{ref} = 2E_{50}^{ref}$. The above reductions were determined by trial so as to receive an end result that was as close as possible to the actual field test results.

The calculation process was the same as described above and its results for the particular phases are presented in Fig. 13–15.

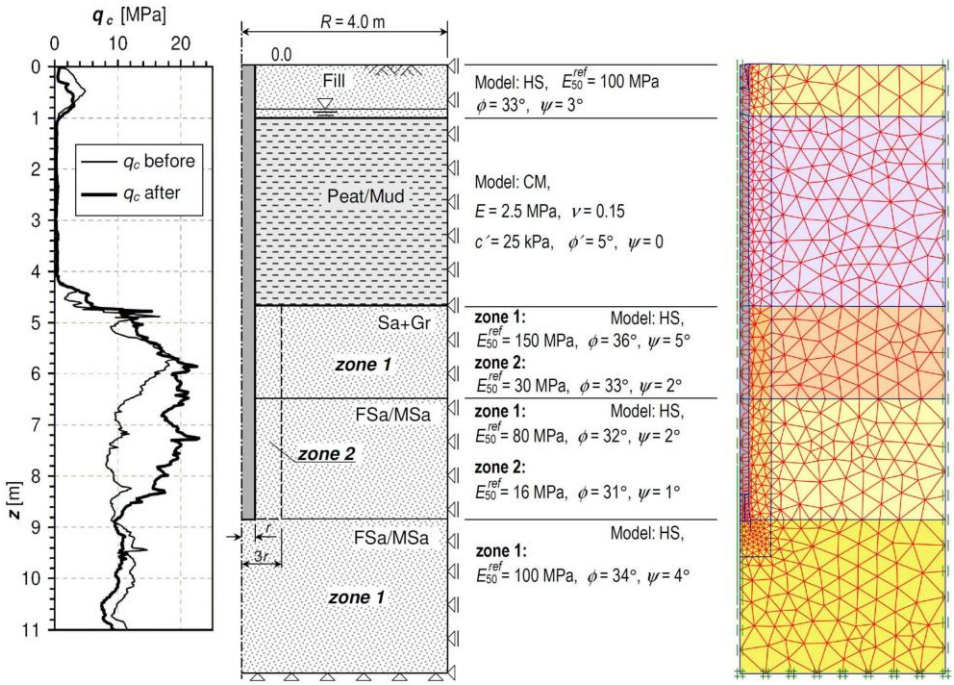

Fig. 12. Geometrical arrangement of zone with adjusted mechanical parameters of soil and discretisation area

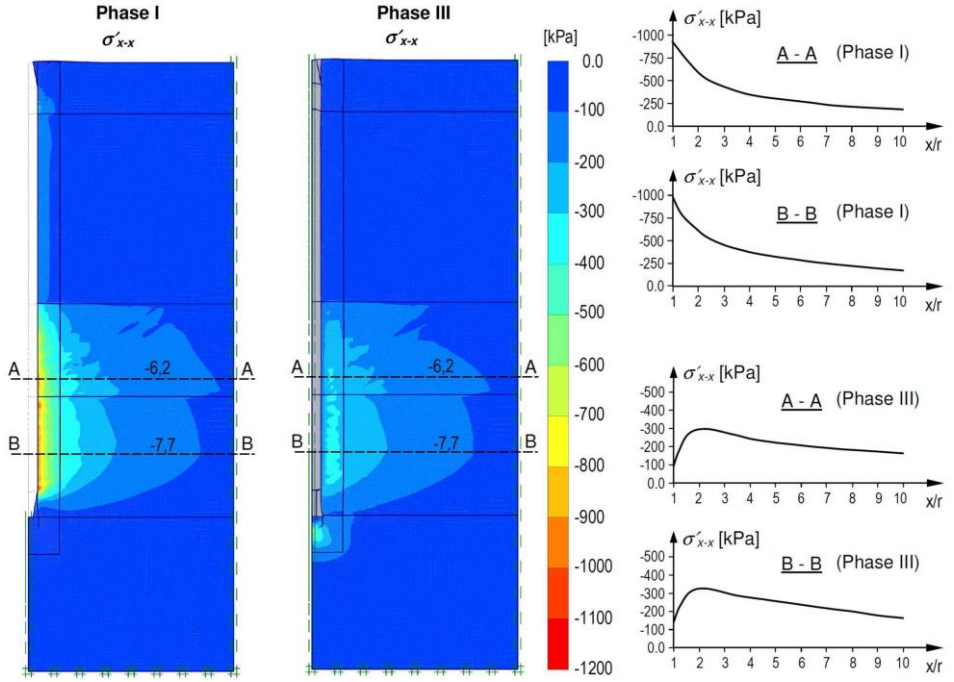

Fig. 13. Phase I and III radial stress distribution in the soil after the second calculation approach

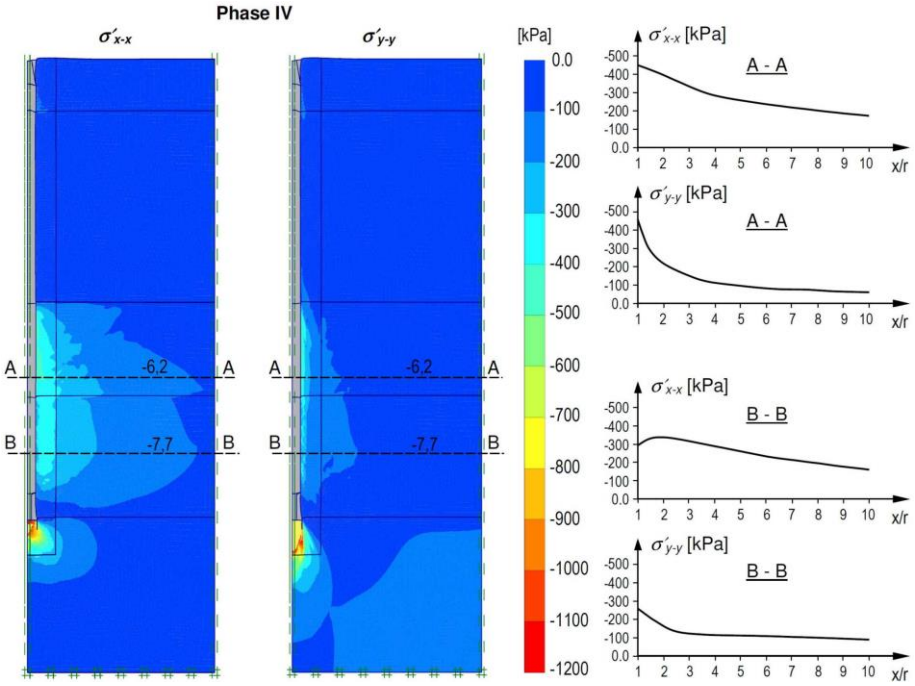

Fig. 14. Phase IV radial and vertical distributions in the soil after the second calculation approach

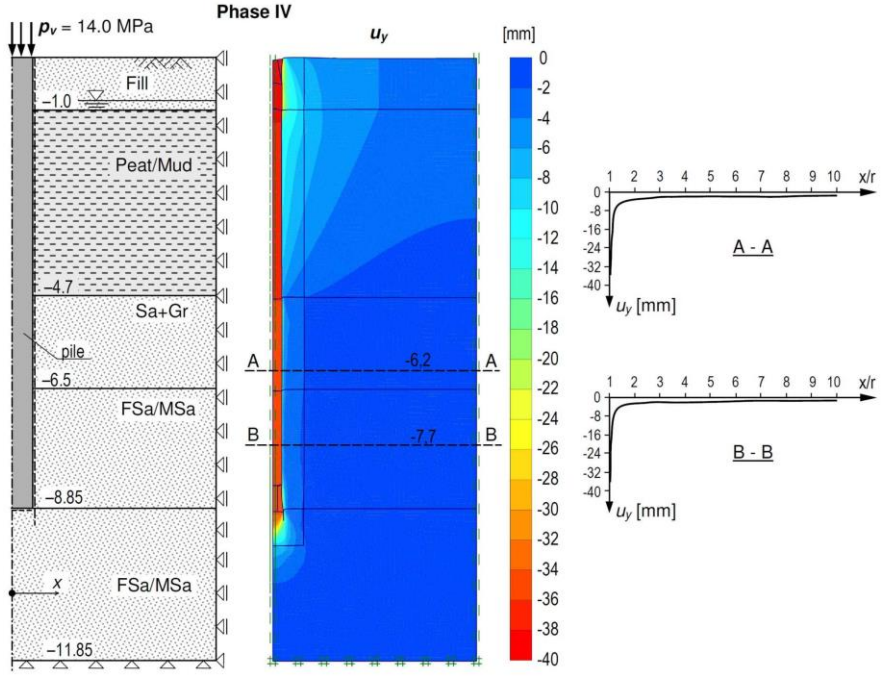

Fig. 15. Phase IV vertical pile and soil displacement field after the second calculation approach

A comparison of the first calculation results with those of the second approach reveals relatively minor differences in phases I, II and III. However, there is a pronounced difference between the results in phase IV (pile load). In the second approach, pile settlement $s \approx 0{,}1D$ only needed a pile head load of p_v = 14.0 MPa, that is some 40% less than in the first approach (p_v = 23.0 MPa).

Fig. 16 presents the load-settlement correlation curves for total force Q and component forces Q_N, Q_s and Q_b obtained from the second approach. Their comparison with field test results is very good.

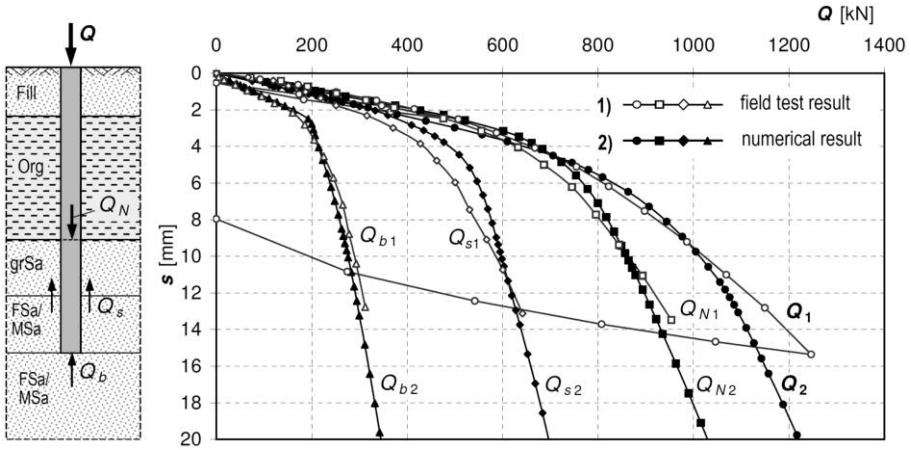

Fig. 16. Pile load-settlement curves from the second approach compared with field test results

7. Conclusions

The examples presented in this article prove that it is possible to numerically model the interaction of a screw displacement pile with non-cohesive soil using a FEM calculation tool such as Plaxis – 2D.

The proposed alternative methods of modelling pile installation phases, particularly the soil displacement phase and pile concreting phase, show good results. The tests have also shown that including these phases has a considerable influence on the final calculation results and therefore should not be left out of the modelling process.

The rotation of the soil displacement auger during cavity formation also has a considerable effect on the final results. A complete omission of its effects causes considerable overestimation in calculations, particularly along the pile shaft. Auger rotation puts the soil around the auger in a critical state, i.e. it reduces its mechanical parameters. Modelling the auger rotation is not possible in an axisymmetric system. Nevertheless, this article has shown that modelling physical rotation is not actually necessary. It is sufficient to take into account the phenomena it causes by reducing the mechanical parameter values of the soil around the pile shaft. The ϕ angle of friction is reduced to ϕ_{cs}, the ψ dilatancy angle to 1–2 ° and soil deformation modulus E to around 20%-30% of its initial value. After the application of these reductions, numerical analysis results correspond well with field test results.

The above numerical analyses confirm field test observations that the load bearing capacity of screw displacement piles is primarily based on shaft resistance Q_s, while the contribution of base resistance Q_b is not very large.

Although the computational approach presented in this article has yielded good results, it may only be treated as a simplified prototype and not the full solution. Further developments regarding the analysis of pile-soil interaction should use an advanced soil model based on

specifically designed laboratory soil tests and pile model tests as well as more sophisticated computational tools to analyse all the soil phenomena represented in the calculation process. Such models and tools have already used, e.g. by Basu and Prezzi [6], but a much more comprehensive approach encompassing the entire pile, from head to base is still necessary.

Acknowledgments

This work was created thanks to research project N N506 432936 financed by the Polish Ministry of Science and Higher Education.

References

[1] M. Bottiau, G. Cortvrindt, Recent experience with the Omega-Pile, DFI, Proc. of 5th Int. Conf. and Exhibition on Piling and Deep Foundations, Bruges, 1994, pp. 3.11.0-3.11.7.

[2] F. De Cock, R. Imbo, Atlas screw pile: a vibration-free, full displacement, cast-in-place pile, Transporation Research Record 1447, 1994, pp. 49-62.

[3] J. Maertens, N. Huybrechts, Belgian screw pile technology. Design and recent developments, Proc. of the Second Symp. on Screw Piles, Brussels, Belgium,. Swets and Zeitlinger B.V., Lisse, The Netherlands, 2003.

[4] K.-P. Mahutka, F. König, J. Grabe, Numerical modelling of pile jacking, driving and vibro driving, Proceedings of International Conference on Numerical Simulation of Construction Processes in Geotechnical Engineering for Urban Environment (NSC06), Bochum, ed. by T. Triantafyllidis, Balkema, Rotterdam, 2006, pp. 235-246.

[5] S. Henke, J. Grabe, Numerical modelling of pile installation, Proc. of 17th Int. Conf. on Soil Mechanics and Foundation Engineering, Alexandria, Egypt, 2009, pp. 1321-1324.

[6] P. Basu, M. Prezzi, Design and Applications of Drilled Displacement (Screw) Piles, Publication FHWA/IN/JTRP-2009/28. Joint Transportation Research Program, Indiana Department of Transportation and Purdue University, West Lafayette, Indiana, 2009. http://docs.lib.purdue.edu/cgi/viewcontent.cgi.

[7] R.B.J. Brinkgreve, Plaxis 2D – Version 8, A.A. Balkema Publishers, Netherlands, 2002.

[8] M. Bustamante, B. Doix, A new model of LCPC removable extensometer, Proc. of the 4th Int. Conf. on Piling and Deep Foundation, Stresa, Italy, 1991.

[9] B.H. Fellenius, From strain measurements to load in an instrumented pile. Geotechnical News Magazine, Vol. 19, No. 1, 2001, pp. 35-38.

[10] J.B. Sellers, Pile load test instrumentation. Instrumentation in Geotechnical Engineering, Proc. of Geotechnical Division of the Hong Kong Institute of Civil Engineers, 1995, pp. 23-33.

[11] A. Krasiński, Advanced field investigations of screw piles and columns, Archives of Civil Engineering, No 1, 2011, pp. 47-57.

[12] A. Krasiński, Badania terenowe przemieszczeniowych pali i kolumn wkręcanych typu SDP i SDC, (in Polish), Drogi i Mosty, Nr 1-2/2011.

[13] A. Krasiński, Wyniki badań terenowych pali i kolumn wkręcanych, (in Polish), Inżynieria Morska i Geotechnika, Nr 6/2011, pp. 510-530.

[14] T. Schanz, P.A. Vermeer, Angles of friction and dilatancy of Sand, Géotechnique 46, 1996, pp. 145-151.

[15] T. Lunne, P. Robertson, J, Powell, Cone penetration testing in Geotechnical Practice, Blackie Academic and Professional, London, 1997.

[16] H.J. Burd H.J., G.T. Houlsby, Analysis cylindrical expansion problems, Int. J. Num. Analys. Mech. Geomech. Vol. 14, 1990, pp. 351-366.

[17] I.F. Collins, M.J. Pender, W. Yan, Cavity expansion in sands under drained loading conditions, International Journal of Numerical and Analytical Methods in Geomechanics, Vol. 16, 1992, No. 1, pp. 3-23.

[18] R. Salgado, M.F. Randolph, Analysis of cavity expansion in sand, Int. Journal of Geomechanics, Vol. 1, No. 2, 2001, pp. 175-192.

[19] M.T. Manzari, Y.F. Dafalias, A critical state two-surface plasticity model for sands, Géotechnique, Vol. 47, No. 2, 1997, pp. 255-272.

[20] P.W. Rowe, The stress-dilatancy relation for static equilibrium of an assembly of particles in contact, Proc. Roy. Soc. A., No. 269,1962, pp. 500-527.

[21] M.D. Bolton, The Strength and Dilatancy of Sands. Géotechnique, Vol. 36, No. 1, 1986, pp 65-78.

[22] J. Biarez, P.-Y Hicher, Elementary Mechanics of Soil Behaviour, Balkema, London, 1994, p. 208.